Published as: *Biophys J*. 2009 July 8; 97(1): 101–109.

Biophysical characterization of styryl dye•membrane interactions

Yao Wu[†], **Felix L. Yeh**[†], **Fei Mao**[‡], and **Edwin R. Chapman**[†,*]

[†] Howard Hughes Medical Institute and Department of Physiology, University of Wisconsin, Madison, WI 53706, USA

[‡] Biotium, Inc., 3423 Investment BLVD, Suite #8, Hayward, CA 94545, USA

Abstract

Styryl dyes (also referred to as FM dyes) become highly fluorescent upon binding to membranes and are often used to study synaptic vesicle recycling in neurons. To date, direct comparisons of the fluorescent properties, or time-resolved (millisecond) measurements of dye•membrane binding and unbinding reactions, for all members of this family of probes, have not been reported. Here, we compare the fluorescence intensities of each member of the FM dye family when bound to membranes; this analysis included SGC5, a new lipophilic fluorescent dye with a unique structure. Fluorescence intensities depended on the length of the lipophilic tail of each dye, with a rank order of: SGC5 > FM1–84 > FM1–43 > SynaptoGreen C3 > FM2–10/FM4–64/FM5–95. Stopped-flow measurements revealed that dye hydrophobicity determined the affinity and departitioning rates for dye•membrane interactions. All of the dyes dissociated from membranes on the millisecond timescale, which is orders of magnitude faster than the overall destaining rate (~s) of these dyes from presynaptic boutons. Departitioning kinetics were faster at higher temperatures, but were unaffected by pH or cholesterol. The data reported here aid interpretation of dye release kinetics from single synaptic vesicles, and indicate that these probes dissociate from membranes on more rapid timescales than previously appreciated.

Keywords

FM dye; exocytosis; kiss-and-run; fusion pore; synaptic vesicle

INTRODUCTION

Pioneering studies by Katz and co-workers established that presynaptic nerve terminals release neurotransmitters in discrete quanta (1). Subsequent studies further confirmed that synaptic vesicles (SVs), loaded with neurotransmitters, gave rise to these quanta by fusing with the presynaptic plasma membrane (2–4). After exocytosis, SVs recycle from the plasma membrane by endocytosis and are reloaded with transmitter for future rounds of transmitter release. Until recently, the synaptic vesicle cycle was largely studied via post-synaptic electrophysiological recordings or by ultrastructural analysis of fixed samples; direct measurements of the synaptic vesicle cycle in intact neurons required the development of new tools to study this process. This need was met in 1992 when Betz, Mao and Bewick characterized a styryl dye - FM1–43

*To whom correspondence should be addressed: Edwin R. Chapman, Howard Hughes Medical, Institute, Department of Physiology, University of Wisconsin, 1300 University Avenue, SMI 129, Madison, WI 53706, E-mail: chapman@physiology.wisc.edu, Tel: (608) 263-1762, Fax: (608) 265-5512.

- which was effectively used to study the synaptic vesicle cycle in the intact neuromuscular junction of frogs (5). Since this groundbreaking study, numerous dyes with slightly different properties have been generated and used to study SV trafficking and to address the idea that there are distinct modes of exocytosis in at least some central synapses (6–11).

In general terms, exocytosis proceeds through a crucial intermediate termed the fusion pore, in which a transient aqueous connection is formed between the vesicle lumen and the extracellular space. Once the fusion pore opens, it has been proposed to have at least two choices, each of which has distinct physiological ramifications (8,12–16). During the well established full fusion pathway, the pore always dilates after opening, resulting in the collapse of the vesicle into the plasma membrane (2,17). In the second putative mode - often referred to as kiss-and-run exocytosis - the fusion pore is thought to undergo a reversal from the open state back to the closed state, which could occur without the complete merger of the vesicle and plasma membrane (18–22). During kiss-and-run exocytosis, the small size of the fusion pore could limit the rate of secretion to potentially drive desensitization, of AMPA receptors for example, rather than activation. Moreover, a small fusion pore could act as a ‘size exclusion filter’, allowing the preferential escape of smaller hormones (e.g., in neuroendocrine cells) while retaining larger hormones which can only be released upon full fusion (23). Kiss-and-run events have been detected via capacitance measurements in the posterior pituitary, chromaffin cells, mast cells, eosinophils, neutrophils, and PC12 cells (15,20,21,24–28), and by amperometric measurements and optical approaches in endocrine and neuroendocrine cells and cell lines (16,21,29–33). However, whether kiss-and-run occurs during synaptic vesicle exocytosis in neurons is a subject of debate (6,10,34–37).

Recent studies have used FM dyes in an attempt to discern between different modes of exocytosis in neurons (6–10). However, interpretation of FM dye destaining experiments requires a detailed understanding of the biophysical properties of the dyes themselves. Which dyes are bright enough to study release from single vesicles? Do the dyes departition from membranes with kinetics that are distinct enough from one another to carry out differential destaining measurements (i.e., full fusion collapse should result in rapid and complete loss of all dyes whereas kiss-and-run should preferentially retain ‘slower’ dyes)? What are the timescales for departitioning versus the open time of a putative kiss-and-run fusion pore?

Earlier studies, in which dye unbinding kinetics were measured via perfusion of cultured neurons, have not resulted in a consensus regarding dye kinetics, and rapid time resolved methods have been applied to only a single dye in the family (FM1–43) (7,38). Therefore, we have carried out detailed biophysical studies of all members of the FM dye family, along with a new dye, SGC5. Here, we report the relative brightness of these dyes, measure their affinities for membranes, and determine the rates at which they bind and unbind from membranes.

MATERIALS AND METHODS

Dyes

FM1–84, FM1–43, FM2–10, FM4–64, and FM5–95 were obtained from Invitrogen (Carlsbad, CA). SynaptoGreen C3 and SGC5 were synthesized by F. Mao (Biotium, Inc.).

Liposomes

1,2-dioleoyl-sn-glycero-3-phosphoethanolamine (PE), 1,2-dioleoyl-sn-glycero-3-phosphocholine (PC), total brain lipid extract, and cholesterol were obtained from Avanti Polar Lipids (Alabaster, AL). Lipids were dissolved in chloroform, dried under nitrogen, and vacuum-lyophilized for one hour. Dried lipid films were then resuspended in HEPES buffer (50 mM HEPES and 100 mM NaCl, pH 7.4). Liposomes composed of total brain lipid were

prepared by sonication (~50 nm) using a Microson ultrasonic cell disruptor (Misonix, Farmingdale, NY). 100 nm liposomes, composed of 30% PE/70% PC, and additional 0%, 5%, 15% and 45% cholesterol, were prepared by extrusion (7,39).

Steady-state fluorescence measurements

Steady-state fluorescence measurements were performed using a PTI QM-1 spectrophotometer (South Brunswick, NJ) at 22°C. Dyes were mixed with liposomes using a castle-style stir bar in a cuvette.

Spectra of dyes after loading into hippocampal neurons

Hippocampal neurons were cultured as previously described (7,40). 14 to 21 day old neurons were loaded with dyes (FM1–84 and SGC5, 2 μM; FM1–43 and FM4–64, 10 μM; SynaptoGreen C3, 20 μM; FM2–10 and FM5–95, 40 μM) in modified Tyrode solution (99 mM NaCl, 55 mM KCl, 2 mM $MgCl_2$, 2 mM $CaCl_2$, 10 mM glucose, 10 mM HEPES, pH7.4) for 3 min at room temperature. Neurons were then washed in calcium free Tyrode solution (150 mM NaCl, 4 mM KCl, 4 mM $MgCl_2$, 0 mM $CaCl_2$, all other components remain unchanged) for 3–10 min. Dye spectra were obtained using an Olympus FV1000 confocal upright microscope with a 488 nm laser to excite the dyes; neurons were imaged with a 60× LUMFL 1.10 water immersion objective (Olympus, Melville, NY). A 405/488 dichroic mirror was used and the emission spectra were collected from 500 nm to 785 nm at 15 nm intervals. Data were collected and analyzed using the Olympus Fluoview 1.7a software.

Stopped-flow rapid mixing experiments

Kinetic experiments were performed using an Applied Photophysics SX 18 MV stopped-flow spectrometer (Leatherhead, Surrey, United Kingdom). Emitted light was collected through a 530 nm cutoff filter. For association experiments, dyes and liposomes were loaded into two different syringes and rapidly mixed (dead time ~1 ms). The final dye concentration was 4 μM. For dissociation experiments, 4 μM dye - bound to membrane (2.2 nM liposomes) - was diluted 1:11 with HEPES buffer. In Fig. 5, *C–I*, the on- (k_{on}) and off-rates (k_{off}) were calculated, assuming pseudo first-order kinetics, according to the following equation: k_{obs} = [liposome] k_{on} + k_{off} (7,38). For departitioning experiments, the rapid fluorescence changes were well fitted by either single, or in some cases double (e.g., FM1–84 and FM1–43), exponential functions. The reason for the second slow component is unclear but might involve the presence of impurities in the dye preparations; this represented a minor component (~10%) of the fluorescence signals. For these reasons, and to simplify comparisons among the different dyes examined, we fit all of the data with single exponential functions.

RESULTS

Quantitative comparison of the fluorescence changes exhibited by FM dyes and SGC5 upon binding to membranes

There are six members of the FM dye family and their structures are shown in Fig. 1. The lipophilic ‘tails’ of these dyes facilitate association with membranes, resulting in a marked increase in fluorescence intensity of the fluorophore core that lies in the middle of each FM dye structure. The spectral properties of these dyes are determined by the two aromatic rings and the connecting double bond in the core region; increasing the number of double bonds in the bridge results in a red shift in the emission spectra (e.g., FM 4–64 and FM 5–95). The other end of the styryl dyes possess a charged ‘head’ which prevent complete insertion into membranes (41).

FM1–84, FM1–43, SynaptoGreen C3, and FM2–10 share an identical fluorophore core. The only difference among this series of dyes lies in the length of their lipophilic tails, and these differences are likely to give rise to different affinities and kinetics for binding to membranes. In this study, we address this issue by comparing the biophysical properties of all six members of the FM dye family, in a side-by-side and quantitative manner, for the first time. In addition, we characterized another new lipophilic fluorescent dye, SGC5 (Fig. 1), which does not belong to FM dye family but has similar fluorescence properties (Fig. 2 and Fig. 4).

As a first step to determine the fluorescence intensity and optimal concentration of the dyes for use in membrane binding experiments, we titrated each dye against a constant concentration of liposomes (2.2 nM liposomes composed of 30% PE/70% PC) (Fig. 2, *B*–*H*). These titrations revealed that FM1–84 was the brightest FM dye, followed by FM1–43 and SynaptoGreen C3; FM2–10, FM4–64, and FM 5–95 were considerably dimmer (Fig. 2 *I*). These results are consistent with the prediction that increases in the lipophilic tail lengths of dyes results in more robust interactions with membranes (i.e., higher affinity binding, deeper insertion into bilayers, or both) and hence greater increases in fluorescence intensity. The novel dye, SGC5, also exhibited strong fluorescence increases upon binding to membranes (Fig. 2, *H* and *I*) and hence should be useful to study synaptic vesicle recycling in neurons as well. SGC5 was therefore included in all experiments to examine the kinetics of dye•membrane interactions.

To determine the optimal concentration of FM dyes for use in cell-based uptake experiments, we used the dye titration data (Fig. 2 *B*–*H*) to calculate the fold enhancement of the fluorescence intensity of each dye upon addition of liposomes (Fig. 2 *J*). FM1–84 exhibited the largest fold-increase upon membrane binding, followed by SGC5 and FM1–43.

To gain a more detailed understanding of the relative intensities and affinities of each dye for membranes, we next titrated increasing [liposome] against a fixed [dye]. FM1–84, FM1–43, and SGC5 exhibited the highest fluorescence intensities, whereas membrane-bound FM2–10, FM4–64, and FM5–95 were, again, relatively dim (Fig. 3 *A*). To facilitate comparisons among the different dyes, we plotted the fold enhancement of the fluorescence intensity of each dye as a function of increasing [liposome]. FM1–84, FM1–43, and SGC5 exhibited the largest fold-increase upon binding to membranes (Fig. 3 *B*), which was consistent with the findings reported in Fig. 2 *J* above, where the dyes were titrated onto a fixed concentration of liposomes.

Since the fluorescence intensity directly reflects the [dye•membrane], the plot shown in Fig. 3 *A* can be used to approximate the relative affinity of the four dyes that share identical fluorophore cores. The rank affinities were: FM1–84>FM1–43>SynaptoGreen C3>FM2–10, and hence coincide with the length of the lipophilic tails in each dye.

To facilitate the utilization/application of the dyes in living cells, we loaded them into recycling synaptic vesicles in cultured hippocampal neurons and determined their emission spectra (Fig. 4 *A*). The emission spectra of FM1–84, FM1–43, SynaptoGreen C3, and FM2–10 were almost identical to one-another, with peak emission wavelengths at ~ 560 nm. The emission spectra of FM4–64 and FM5–95 were also similar to one-another, with red-shifted with emission peaks (relative to all the other dyes) at ~ 635 nm. Finally, the emission peak of SGC5 was ~ 530 nm (Fig. 4 *A*). There was no significant fluorescence emission beyond 700 nm for any of the dyes tested. When compared to the spectra of dyes bound to 30% PE/70% PC liposomes (as well as the spectra provided by the vendor), the emission spectra of dyes loaded in cultured hippocampal neurons were all slightly blue shifted (Fig. 4 *B*), which is likely due to differences in the local environment of the fluorophore cores of each dye (e.g. differences in membrane composition, the presence or absence of proteins etc.).

Kinetics of dye•membrane interactions: effect of temperature, pH and lipid composition

To determine the kinetics of FM dye•membrane binding and unbinding reactions, we performed stopped-flow rapid mixing experiments (Fig. 5 *A* and 6 *A*). For association experiments, dyes were kept constant at 4 μM, and the [liposome] (30% PE/70% PC was varied from 1.1–5.5 nM (Fig. 5, *C* and *D*) or 3.3–7.7 nM (Fig. 5, *E–I*). Upon mixing, a rapid increase in fluorescence intensity - due to dye•membrane complexes formation - was observed (Fig. 5, *A* and *B*). The observed rate constants, k_{obs}, were calculated by fitting the fluorescence traces with single exponential functions (Fig. 5 *B*) and are plotted versus [liposome] in Fig. 5, *C–I*. The rate constants, k_{on} and k_{off}, were obtained from these plots as described in Materials and Methods and these data are shown in Table 1. The resultant dissociation constants (K_d; calculated from k_{off}/k_{on}) indicate that the order of affinity, from high to low, was: FM1–84, FM1–43, SynaptoGreen C3, and FM2–10. This rank order is consistent with the steady state experiments in Fig. 3, and is also consistent with the relative hydrophobicity of each dye; longer and thus more hydrophobic tails result in higher affinity binding.

For rapid departitioning experiments, dyes (4 μM) were premixed with liposomes (2.2 nM; 30% PE/70% PC) in small syringe of the stopped-flow spectrometer, and then rapidly mixed with buffer from a large syringe resulting in a 1:11 dilution. Averaged dilution traces are shown in Fig. 6, where the fluorescence signals dropped to a new baseline within several to tens of milliseconds. These rapid fluorescence changes were fitted by single exponential functions (Table 1) as described in Materials and Methods. FM1–84 dissociated from membranes with the slowest kinetics, whereas FM2–10 departitioned with the fastest kinetics. These differences are due to the different length tails of these dyes, as they share the same fluorophore core structure. The new dye, SGC5 exhibited an intermediate rate of departitioning. In rapid departitioning experiments, $k_{off} \gg k_{on}$, so $k_{diss} \approx k_{off}$, and comparisons between the k_{off} and k_{diss} (Table 1) data generated here reveal good overall agreement (the k_{diss} values are somewhat slower than k_{off} when k_{on} has been neglected).

To quantify the effect of temperature on dye departitioning kinetics, we picked the three brightest dyes, FM1–43, FM1–84, and SGC5, and performed rapid dilution experiments at different temperatures (from 6°C to 37°C) (Fig. 7 *A*). Moreover, because there is a pH gradient across the vesicle membrane in cells, we assayed the rates of departitioning of these three dyes at different pH values (from 5.4 to 7.4), once again using a rapid mixing stopped-flow approach (Fig. 7 *B*). As expected, the departitioning kinetics became faster at higher temperature, but the rank order of rates remained constant (Fig. 7 *A*). However, the kinetics of departitioning were unaffected by pH (Fig. 7 *B*); hence differences in vesicle lumen pH in living cells is unlikely to confound interpretation of FM destaining experiments using neurons.

Finally, we tested the influence of lipid composition on the departitioning kinetics of FM1–43 and FM1–84. For these experiments, we generated liposomes composed of total brain lipid, or 30% PE/70% PC with increasing amounts of cholesterol to systematically influence membrane fluidity. We note that the molar ratio of cholesterol/phospholipid in synaptic vesicles and synaptosomal membranes is ~45% of the total lipid (42,43). Therefore, we included 5%, 15% and 45% cholesterol (cholesterol/phospholipid) in PE/PC vesicles. In all cases, the departitioning kinetics of FM1–84 were slower than for FM1–43. Inclusion of cholesterol did not affect the departitioning kinetics of either dye. However, FM1–43 and FM1–84 dissociated more slowly from vesicles made from total lipid extract derived from brain, but these rates still remained on the ms timescale (Fig. 7, *C* and *D*).

DISCUSSION

In the present work, we have compared the biophysical properties of all members of the FM dye family to gain a better understanding of how these probes interact with membranes. We

first monitored fluorescence changes as a function of the [dye] and [liposome] to help determine the optimal concentrations of each dye for use in membrane staining experiments and to gain qualitative insights into the relative affinity of each dye. This analysis included a new dye, SGC5, that we show engages membrane akin to the FM dyes (Table 1) and becomes highly fluorescent upon inserting into lipid bilayers (Fig. 2, *H–J*, and 3 *A*). These experiments revealed that FM1–43, FM1–84 and SGC5, had the highest fluorescence intensities (Fig. 2 *I* and 3 *A*) and the greatest signal/noise ratios (Fig. 2 *J* and 3 *B*). Hence, this subgroup of dyes are the most promising candidates to study single synaptic vesicles (7,9,10,34,44).

We also measured the emission spectra of each dye after loading them into presynaptic nerve terminals (Fig. 4 *A*), and found that these spectra differ from the spectra obtained using artificial liposomes and also differ from the spectra provided by the vendor. However, these experiments confirmed that the emission spectra of FM4–64 and FM5–95 exhibited a significant red-shift, as compared to other dyes (Fig. 4 *A*). The distinct red shifted spectra of these two dyes has make them particularly useful for two color imaging studies, in conjugation with Qdots (45), or green fluorescent protein (33,46–48).

In addition to the steady state characterization of the dyes, we also determined the kinetics of dye•membrane binding and unbinding reactions using a stopped-flow rapid mixing approach (Fig. 5 *A* and 6 *A*). This approach is more sensitive to changes in fluorescence intensity as compared to cell-based experiments and has the advantage of much higher time resolution (dead time ~ 1 ms). From our time-resolved dye•membrane association experiments, we obtained k_{on} and k_{off} for each dye, and we used these values to calculate K_d for binding (Table 1). Among the four dyes that have identical fluorophore cores, the relative affinities, from high to low, were: FM1–84, FM1–43, SynaptoGreen C3, and FM2–10. The on-rates (k_{on}) were similar for all four of these dyes, but the off-rate (k_{off}) for FM1–84 was significantly slower as compared to the other three dyes, whose k_{off} values were in the similar range. It may be possible that, compared to the shorter tails of the other dyes, the 5-carbon tails of FM1–84 may have reached a critical length that results in significantly greater hydrophobic interaction between the dye and lipids such that there is a greater energy barrier for FM1–84 to overcome during departitioning from membranes (Fig. 1). This finding was further supported by the k_{diss} data (Table 1) demonstrating that FM1–84 dissociates from membranes with slower kinetics than the other dyes that possess the same core structure.

Rapid departitioning experiments revealed that all of the FM dyes, as well as SGC5, dissociate from membranes on the ~ms timescale (Table 1), which is much faster than previously reported using live cell perfusion assays (~s) (8,49,50). We note that in rapid departitioning experiments, $k_{off} \gg k_{on}$, so $k_{diss} \approx k_{off}$, and the differences between k_{off} and k_{diss} increase with larger k_{on} values (e.g., FM1–84 and FM1–43) (Table 1). So, the measurements of both k_{off} and k_{diss} reported here support the conclusion that FM dyes and SGC5 unbind from membranes with much faster kinetics than previously thought.

As expected, we found that the rate of dye departitioning from membranes became faster at higher temperatures (Fig. 7 *A*), but not when membrane fluidity was varied by changing the level of cholesterol (Fig. 7, *C* and *D*). These findings provide support for the notion that membrane composition has limited effects on the kinetics of dye binding and unbinding reactions (7). However, we did observe a ~2-fold reduction in the rate of dye departitioning when vesicles were composed of total brain lipid versus vesicles composed of the two major phospholipids in cells, PE and PC (Fig. 7, *C* and *D*), but departitioning was still rapid. It is possible that the +2 charge in the dye 'head' participates in electrostatic interactions that retard dissociation from membranes that harbor anionic phospholipids. Finally, the rates of departitioning appear to be independent of pH; similar rates of dissociation were observed from

pH 5.4 to pH 7.4. These data suggest that differences in intravesicular pH are unlikely to confound the analysis of single vesicle destaining data (Fig. 7 *B*).

The data reported here and in ref. (7) demonstrate that the kinetics of FM dye departitioning from membranes (~ms) (Table 1) are orders of magnitude faster than the overall destaining rates from presynaptic nerve terminals (~s) (7,8,49,51). Synaptic vesicles, labeled with dyes via prior exo- and endocytosis, must transit through multiple steps before undergoing re-release, and these kinetic differences reflect, in part, these processes. Other factors also affect the rate at which dyes are lost from labeled nerve terminals during exocytosis, including re-binding to the plasma membrane after release and trapping of dyes in synaptic structures. In addition, it is possible that some events occur via non-dilating kiss-and-run fusion pores that retard the rate of dye efflux (7). Related to this point are the findings that different FM dyes (e.g., FM1–84, FM1–43, and FM2–10) are released from pre-synaptic boutons at different rates (8) (but see also ref. (49–51)). Since, as shown in the current study, these dyes leave membranes with similar rapid kinetics, why do they destain from boutons with distinct kinetics? This puzzle points back to the notion that some release events are mediated by nm-scale pores. Since the axial diameter of the FM dyes are similar to the diameter of fusion pores that have been measured directly in a variety of cell types that secrete hormones, transmitters, and other factors (12,15,16,20,21,24–27,29,52–55), small changes in the diameter of the dyes could have significant effects on the rate of efflux through small, non-dilating, fusion pores. Future studies, focusing on the dimensions of these dyes and the rates at which they flux through defined pores in membranes (7) - rather than their membrane departitioning kinetics - are underway and should shed light on these questions.

Acknowledgments

We thank J. Bai and the Chapman lab for helpful discussions. This work was supported by grants from the AHA (0440168N) and NIH (MH 61876). E.R.C is an Investigator of the Howard Hughes Medical Institute.

References

1. Del Castillo J, Katz B. Quantal components of the end-plate potential. J Physiol 1954;124:560–573. [PubMed: 13175199]
2. Heuser JE, Reese TS. Evidence for recycling of synaptic vesicle membrane during transmitter release at the frog neuromuscular junction. J Cell Biol 1973;57:315–344. [PubMed: 4348786]
3. Maycox PR, Link E, Reetz A, Morris SA, Jahn R. Clathrin-coated vesicles in nervous tissue are involved primarily in synaptic vesicle recycling. J Cell Biol 1992;118:1379–1388. [PubMed: 1325974]
4. Farsad K, De Camilli P. Neurotransmission and the synaptic vesicle cycle. Yale J Biol Med 2002;75:261–284. [PubMed: 14580108]
5. Betz WJ, Mao F, Bewick GS. Activity-dependent fluorescent staining and destaining of living vertebrate motor nerve terminals. J Neurosci 1992;12:363–375. [PubMed: 1371312]
6. Harata NC, Aravanis AM, Tsien RW. Kiss-and-run and full-collapse fusion as modes of exo-endocytosis in neurosecretion. J Neurochem 2006;97:1546–1570. [PubMed: 16805768]
7. Richards DA, Bai J, Chapman ER. Two modes of exocytosis at hippocampal synapses revealed by rate of FM1–43 efflux from individual vesicles. J Cell Biol 2005;168:929–939. [PubMed: 15767463]
8. Klingauf J, Kavalali ET, Tsien RW. Kinetics and regulation of fast endocytosis at hippocampal synapses. Nature 1998;394:581–585. [PubMed: 9707119]
9. Aravanis AM, Pyle JL, Harata NC, Tsien RW. Imaging single synaptic vesicles undergoing repeated fusion events: kissing, running, and kissing again. Neuropharmacology 2003;45:797–813. [PubMed: 14529718]
10. Aravanis AM, Pyle JL, Tsien RW. Single synaptic vesicles fusing transiently and successively without loss of identity. Nature 2003;423:643–647. [PubMed: 12789339]

11. Harata NC, Choi S, Pyle JL, Aravanis AM, Tsien RW. Frequency-dependent kinetics and prevalence of kiss-and-run and reuse at hippocampal synapses studied with novel quenching methods. Neuron 2006;49:243–256. [PubMed: 16423698]
12. Ales E, Tabares L, Poyato JM, Valero V, Lindau M, Alvarez de Toledo G. High calcium concentrations shift the mode of exocytosis to the kiss-and-run mechanism. Nat Cell Biol 1999;1:40–44. [PubMed: 10559862]
13. Neher E, Marty A. Discrete changes of cell membrane capacitance observed under conditions of enhanced secretion in bovine adrenal chromaffin cells. Proc Natl Acad Sci U S A 1982;79:6712–6716. [PubMed: 6959149]
14. Stevens CF, Williams JH. "Kiss and run" exocytosis at hippocampal synapses. Proc Natl Acad Sci U S A 2000;97:12828–12833. [PubMed: 11050187]
15. Klyachko VA, Jackson MB. Capacitance steps and fusion pores of small and large-dense-core vesicles in nerve terminals. Nature 2002;418:89–92. [PubMed: 12097912]
16. Wang CT, Lu JC, Bai J, Chang PY, Martin TF, Chapman ER, Jackson MB. Different domains of synaptotagmin control the choice between kiss-and-run and full fusion. Nature 2003;424:943–947. [PubMed: 12931189]
17. Heuser JE. Review of electron microscopic evidence favouring vesicle exocytosis as the structural basis for quantal release during synaptic transmission. Q J Exp Physiol 1989;74:1051–1069. [PubMed: 2560556]
18. Ceccarelli B, Hurlbut WP, Mauro A. Turnover of transmitter and synaptic vesicles at the frog neuromuscular junction. J Cell Biol 1973;57:499–524. [PubMed: 4348791]
19. Fesce R, Grohovaz F, Valtorta F, Meldolesi J. Neurotransmitter release: fusion or 'kiss-and-run'? Trends Cell Biol 1994;4:1–4. [PubMed: 14731821]
20. Lindau M, Almers W. Structure and function of fusion pores in exocytosis and ectoplasmic membrane fusion. Curr Opin Cell Biol 1995;7:509–517. [PubMed: 7495570]
21. Jackson MB, Chapman ER. Fusion pores and fusion machines in Ca2+-triggered exocytosis. Annu Rev Biophys Biomol Struct 2006;35:135–160. [PubMed: 16689631]
22. Jackson MB, Chapman ER. The fusion pores of Ca(2+)-triggered exocytosis. Nat Struct Mol Biol 2008;15:684–689. [PubMed: 18596819]
23. Fulop T, Radabaugh S, Smith C. Activity-dependent differential transmitter release in mouse adrenal chromaffin cells. J Neurosci 2005;25:7324–7332. [PubMed: 16093382]
24. Monck JR, Alvarez de Toledo G, Fernandez JM. Tension in secretory granule membranes causes extensive membrane transfer through the exocytotic fusion pore. Proc Natl Acad Sci U S A 1990;87:7804–7808. [PubMed: 2235997]
25. Hartmann J, Lindau M. A novel Ca(2+)-dependent step in exocytosis subsequent to vesicle fusion. FEBS Lett 1995;363:217–220. [PubMed: 7737405]
26. Lollike K, Borregaard N, Lindau M. The exocytotic fusion pore of small granules has a conductance similar to an ion channel. J Cell Biol 1995;129:99–104. [PubMed: 7535305]
27. Spruce AE, Breckenridge LJ, Lee AK, Almers W. Properties of the fusion pore that forms during exocytosis of a mast cell secretory vesicle. Neuron 1990;4:643–654. [PubMed: 2344404]
28. Fernandez JM, Neher E, Gomperts BD. Capacitance measurements reveal stepwise fusion events in degranulating mast cells. Nature 1984;312:453–455. [PubMed: 6504157]
29. Albillos A, Dernick G, Horstmann H, Almers W, Alvarez de Toledo G, Lindau M. The exocytotic event in chromaffin cells revealed by patch amperometry. Nature 1997;389:509–512. [PubMed: 9333242]
30. Alvarez de Toledo G, Fernandez-Chacon R, Fernandez JM. Release of secretory products during transient vesicle fusion. Nature 1993;363:554–558. [PubMed: 8505984]
31. Wang CT, Bai J, Chang PY, Chapman ER, Jackson MB. Synaptotagmin-Ca2+ triggers two sequential steps in regulated exocytosis in rat PC12 cells: fusion pore opening and fusion pore dilation. J Physiol 2006;570:295–307. [PubMed: 16293646]
32. Tsuboi T, Rutter GA. Multiple forms of "kiss-and-run" exocytosis revealed by evanescent wave microscopy. Curr Biol 2003;13:563–567. [PubMed: 12676086]

33. Taraska JW, Almers W. Bilayers merge even when exocytosis is transient. Proc Natl Acad Sci U S A 2004;101:8780–8785. [PubMed: 15173592]
34. Balaji J, Ryan TA. Single-vesicle imaging reveals that synaptic vesicle exocytosis and endocytosis are coupled by a single stochastic mode. Proc Natl Acad Sci U S A 2007;104:20576–20581. [PubMed: 18077369]
35. Gandhi SP, Stevens CF. Three modes of synaptic vesicular recycling revealed by single-vesicle imaging. Nature 2003;423:607–613. [PubMed: 12789331]
36. He L, Wu XS, Mohan R, Wu LG. Two modes of fusion pore opening revealed by cell-attached recordings at a synapse. Nature 2006;444:102–105. [PubMed: 17065984]
37. Granseth B, Odermatt B, Royle SJ, Lagnado L. Clathrin-mediated endocytosis is the dominant mechanism of vesicle retrieval at hippocampal synapses. Neuron 2006;51:773–786. [PubMed: 16982422]
38. Neves G, Lagnado L. The kinetics of exocytosis and endocytosis in the synaptic terminal of goldfish retinal bipolar cells. J Physiol 1999;515(Pt 1):181–202. [PubMed: 9925888]
39. Davis AF, Bai J, Fasshauer D, Wolowick MJ, Lewis JL, Chapman ER. Kinetics of synaptotagmin responses to Ca2+ and assembly with the core SNARE complex onto membranes. Neuron 1999;24:363–376. [PubMed: 10571230]
40. Dong M, Yeh F, Tepp WH, Dean C, Johnson EA, Janz R, Chapman ER. SV2 is the protein receptor for botulinum neurotoxin A. Science 2006;312:592–596. [PubMed: 16543415]
41. Gaffield MA, Betz WJ. Imaging synaptic vesicle exocytosis and endocytosis with FM dyes. Nat Protoc 2006;1:2916–2921. [PubMed: 17406552]
42. Westhead EW. Lipid composition and orientation in secretory vesicles. Ann N Y Acad Sci 1987;493:92–100. [PubMed: 3473971]
43. Breckenridge WC, Gombos G, Morgan IG. The lipid composition of adult rat brain synaptosomal plasma membranes. Biochim Biophys Acta 1972;266:695–707. [PubMed: 4339171]
44. Chen X, Barg S, Almers W. Release of the styryl dyes from single synaptic vesicles in hippocampal neurons. J Neurosci 2008;28:1894–1903. [PubMed: 18287506]
45. Zhang Q, Cao YQ, Tsien RW. Quantum dots provide an optical signal specific to full collapse fusion of synaptic vesicles. Proc Natl Acad Sci U S A 2007;104:17843–17848. [PubMed: 17968015]
46. Cai Q, Pan PY, Sheng ZH. Syntabulin-kinesin-1 family member 5B-mediated axonal transport contributes to activity-dependent presynaptic assembly. J Neurosci 2007;27:7284–7296. [PubMed: 17611281]
47. Chi P, Greengard P, Ryan TA. Synapsin dispersion and reclustering during synaptic activity. Nat Neurosci 2001;4:1187–1193. [PubMed: 11685225]
48. Santos MS, Barbosa J Jr, Veloso GS, Ribeiro F, Kushmerick C, Gomez MV, Ferguson SS, Prado VF, Prado MA. Trafficking of green fluorescent protein tagged-vesicular acetylcholine transporter to varicosities in a cholinergic cell line. J Neurochem 2001;78:1104–1113. [PubMed: 11553684]
49. Ryan TA, Smith SJ, Reuter H. The timing of synaptic vesicle endocytosis. Proc Natl Acad Sci U S A 1996;93:5567–5571. [PubMed: 8643616]
50. Richards DA, Guatimosim C, Betz WJ. Two endocytic recycling routes selectively fill two vesicle pools in frog motor nerve terminals. Neuron 2000;27:551–559. [PubMed: 11055437]
51. Fernandez-Alfonso T, Ryan TA. The kinetics of synaptic vesicle pool depletion at CNS synaptic terminals. Neuron 2004;41:943–953. [PubMed: 15046726]
52. Han X, Wang CT, Bai J, Chapman ER, Jackson MB. Transmembrane segments of syntaxin line the fusion pore of Ca2+-triggered exocytosis. Science 2004;304:289–292. [PubMed: 15016962]
53. Breckenridge LJ, Almers W. Currents through the fusion pore that forms during exocytosis of a secretory vesicle. Nature 1987;328:814–817. [PubMed: 2442614]
54. Debus K, Lindau M. Resolution of patch capacitance recordings and of fusion pore conductances in small vesicles. Biophys J 2000;78:2983–2997. [PubMed: 10827977]
55. Wang CT, Grishanin R, Earles CA, Chang PY, Martin TF, Chapman ER, Jackson MB. Synaptotagmin modulation of fusion pore kinetics in regulated exocytosis of dense-core vesicles. Science 2001;294:1111–1115. [PubMed: 11691996]

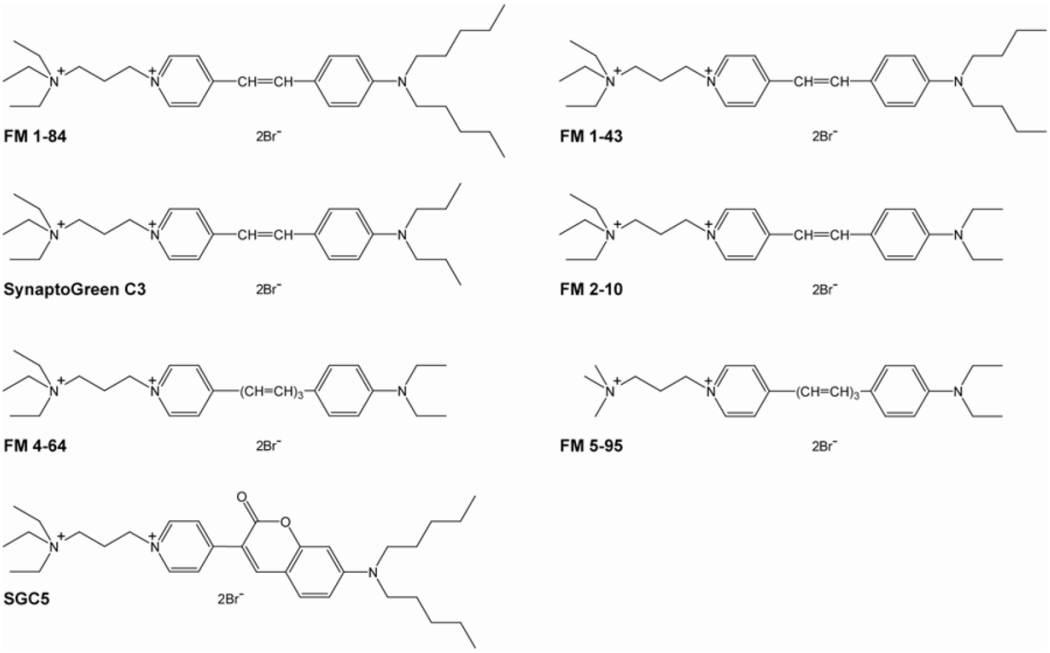

FIGURE 1. Dye structures

FM1–84, FM1–43, SynaptoGreen C3 and FM2–10 share identical fluorophore cores. All of the FM dyes have two lipophilic ‘tails’; in FM1–84, the lipophilic tails are composed of 4 methylene groups and a terminal methyl group. FM1–43, SynaptoGreen C3, and FM 2–10 have hydrocarbon tails composed of 4, 3, and 2 carbons, respectively. FM 4–64 and FM 5–95 have the same two-carbon tails but have distinct charged ‘head’ regions.

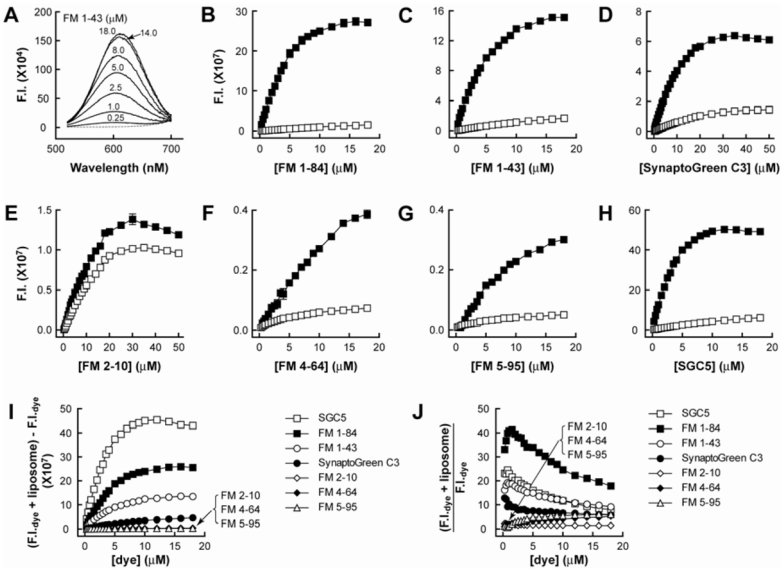

FIGURE 2. Fluorescence intensity of dye•membrane complexes as a function of increasing dye concentration

(*A*) Titration of liposomes (2.2 nM liposomes composed of 30% PE/70% PC) against [FM1–43]. The dashed line represents the signal obtained from liposomes only, and the solid lines are liposomes plus the indicated [FM1–43]. (*B–H*) Fluorescence intensities, determined by integration of emission spectra of dye•liposome complexes (500–700 nm for FM1–84, FM1–43, SynaptoGreen C3, and FM2–10; 550–750 nm for FM4–64 and FM5–95; 500–650 nm for SGC5), are indicated by solid squares. Fluorescence intensities of samples that contained dyes but lacked liposomes are indicated by open squares. (*I*) Dye•liposome fluorescence intensities were corrected by subtracting the free dye signals; these data are plotted versus [dye]. (*J*) Ratio of fluorescence intensities of dyes with and without liposomes. Error bars are mean ± SE from three separate experiments.

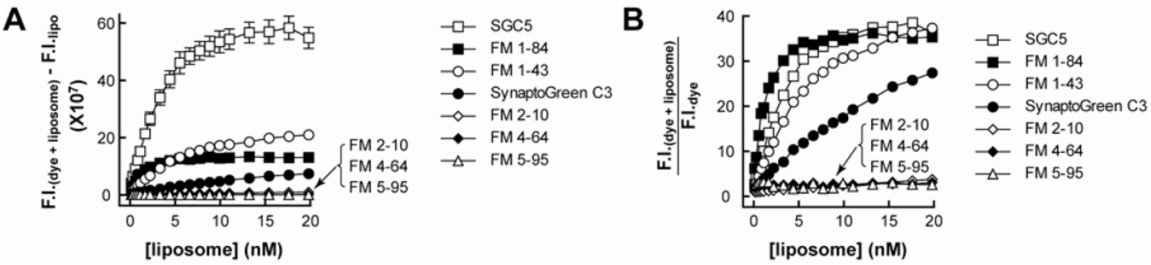

FIGURE 3. Fluorescence intensity of dye•membrane complexes as a function of liposome concentration

(*A*) Increase in the fluorescence intensity of a fixed concentration of each dye as a function of increasing [liposome] (30% PE/70% PC); data were corrected by subtracting signals obtained from liposome-alone samples. EC_{50} values, which approximate the affinities of the dyes for membranes, were determined for the three brightest dyes: SGC5, FM1–84, and FM1–43, and these values were 4.0, 1.3, and 4.2 nM respectively. These values are in reasonable agreement with the dissociation constants determined by the kinetic experiments described in Fig. 5 below and in Table 1. (*B*) Ratio of fluorescence intensities of all of the dyes tested; SGC5, FM1–84, and FM1–43 yielded the highest signal-to-background ratios. Error bars are mean ± SE from three independent experiments.

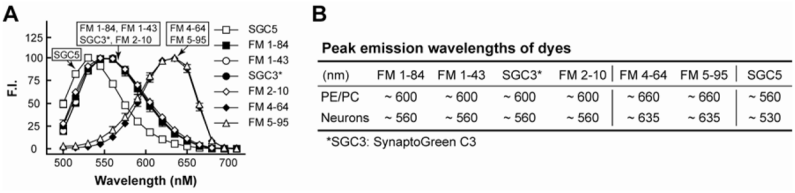

FIGURE 4. Spectra of dyes after loading into hippocampal neurons

(*A*) Emission spectra from hippocampal neurons loaded with 2 μM SGC5 (open squares), 2 μM FM1–84 (solid squares), 10 μM FM1–43 (open circles), 20 μM SynaptoGreen C3 (solid circles), 40 μM FM2–10 (open diamonds), 10 μM FM4–64 (solid diamonds), or 40 μM FM5–95 (open triangles) were background corrected and normalized. Error bars are standard deviations (n = 27). (*B*) Peak emission wavelengths of dyes bound to liposomes (30% PE/70% PC) or loaded into cultured hippocampal neurons.

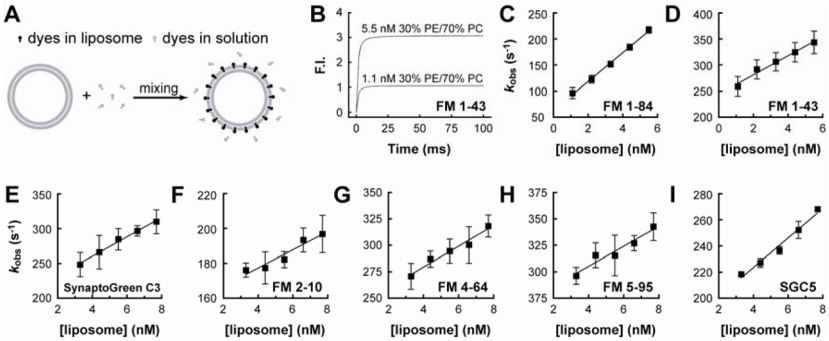

FIGURE 5. Binding and unbinding kinetics of dye•membrane interactions

(*A*) Outline of the experimental procedure used to measure the association of dyes with membranes. Dye and liposomes (30% PE/70% PC) were rapidly mixed in a stopped-flow spectrometer at a 1:1 volume ratio; binding results in a marked increase in fluorescence intensity. (*B*) Representative traces of the fluorescence increases that occur upon mixing dyes with two concentrations of liposomes. The traces can be well fitted using single exponential functions and the rate, k_{obs}, determined. (*C–I*) The observed rates, k_{obs}, were plotted as a function of [liposome]. The rate constants, k_{on} and k_{off}, were obtained from these plots by assuming pseudo first order kinetics as detailed in Materials and Methods. The dissociation constants, K_d, were determined from k_{off}/k_{on} (Table 1). Error bars represent mean ± SE from three independent determinations.

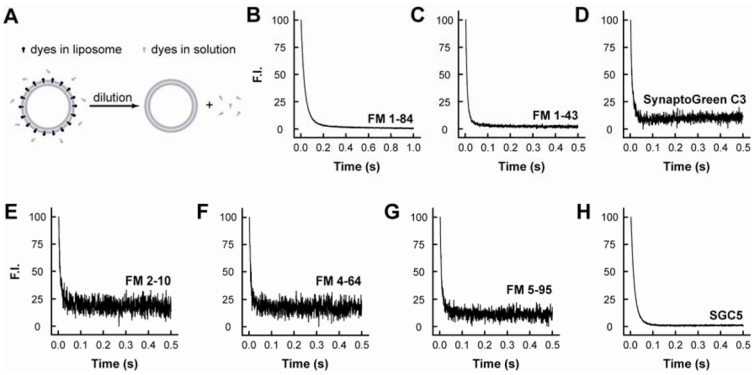

FIGURE 6. Departitioning kinetics of dye•membrane complexes

(*A*) Outline of the experimental procedure used to measure departitioning kinetics. Dye/liposome mixtures were rapidly diluted (1:11); as membrane-bound dyes dissociate, the fluorescence intensity decreases. (*B–H*) Representative traces, and exponential fits, showing the rate of dye dissociation from membranes.

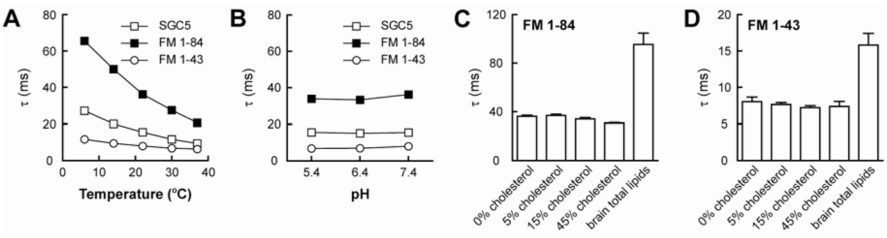

FIGURE 7. Departitioning kinetics of dye•membrane complexes as a function of temperature, pH and membrane composition

Departitioning kinetics of dye•membrane complexes at the indicated temperature (*A*), pH (*B*), or vesicle composition (*C* and *D*). In panels *C* and *D*, the vesicle composition was 30% PE/70% PC with increasing amounts of cholesterol (cholesterol/phospholipid ratios: 0%, 5%, 15%, and 45%). Departitioning was monitored by dilution in a stopped-flow spectrometer; the fluorescence decreases were fit with single exponential functions, and the time constants plotted.

TABLE 1

Kinetics of dye association and departitioning with liposomes

(30% PE/70% PC, diameter: 100 nm, pH 7.4, 22.0°C)

	FM 1–84	FM 1–43	SynaptoGreen C3	FM 2–10	FM 4–64	FM 5–95	SGC5
k_{on} (nM^{-1} s^{-1})	28 ± 2	18 ± 5	14 ± 4	5 ± 2	10 ± 3	9 ± 3	11 ± 1
k_{off} (s^{-1})	63 ± 7	245 ± 18	204 ± 25	157 ± 30	240 ± 32	251 ± 28	178 ± 6
K_d (*nM*)	2.3	13.3	14.6	30.0	24.3	26.5	15.8
k_{diss} (s^{-1})	28 ± 1	126 ± 9	149 ± 22	174 ± 35	129 ± 20	131 ± 18	64 ± 2
τ_{diss} (*ms*)	36.3 ± 0.9	8.0 ± 0.6	7.0 ± 0.9	6.4 ± 1.8	8.1 ± 1.2	7.9 ± 1.0	15.5 ± 0.4